RSC Advances

PAPER

View Article Online
View Journal | View Issue

Cite this: *RSC Adv.*, 2016, **6**, 17995

A chemosensor for Al^{3+} ions in aqueous ethanol media: photophysical and live cell imaging studies†

Nabanita Chatterjee,[a] Shubhra Bikash Maity,[a] Asmita Samadder,[bc] Puspal Mukherjee,[a] Anisur Rahman Khuda-Bukhsh[b] and Parimal K. Bharadwaj*[a]

Received 13th November 2015
Accepted 26th January 2016

DOI: 10.1039/c5ra23968k

www.rsc.org/advances

A novel fluorescent chemosensor **L** has been designed and synthesized based on the rhodamine-B moiety. The dye **L** exhibits selective fluorescence enhancement towards the Al^{3+} ion over other biologically relevant metal ions in aqueous ethanolic media (EtOH–H_2O, 2 : 3, v/v). The structure of the probe **L** has been established by ^1H and ^{13}C-NMR spectroscopy, single crystal X-ray diffraction, ESI-mass spectrometry and elemental analysis. The cleavage of the spirolactam bond of the rhodamine moiety induced by the Al^{3+} ion generates the delocalized xanthene fluorophore that is responsible for the emission enhancement of the probe **L**. The recognition behavior of the receptor **L** has been investigated experimentally with supports from theoretical DFT studies. Furthermore, the efficacy of **L** in cell imaging studies is also probed by confocal microscopy.

Introduction

The design and synthesis of fluorescent probes for environmentally hazardous metal ions has achieved considerable recent interest in terms of using these probes for chemosensing, live cell imaging, ion transport, metalloenzyme mimics, catalysis and nuclear waste treatment.[1–3] Extensive use of aluminum in food additives, pharmaceuticals, electrical equipment, cooking utensils, computer parts *etc.*[4] leads to environmental problems. In humans, it exists[5] in its ionic form Al^{3+} with a long residence time before excretion through urine. Accumulation of this ion can be potentially hazardous affecting neurological order that may lead to Parkinson's disease, Alzheimer's disease *etc.*[6,7] It also hampers the growth of plants and biological functions of metalloenzymes.[8] Therefore, spatial as well as temporal distribution of Al^{3+} ions even at low concentration is highly desirable.

Our interest in developing chemosensors for the Al^{3+} ion led us to synthesize the dye **L** to utilize the excellent photophysical properties of rhodamine B as a turn-on sensor.[9–11] Several rhodamine derivatives have been reported as sensors for the Al^{3+} ions.[12–17] Most of them are functional only in organic solvents due to strong hydration of Al^{3+} in water thus making them difficult for practical applications.[18] To increase aqueous solubility of the chemosensor, 2-methoxy-4-nitroaniline group, has been appended as the receptor to the rhodamine B moiety (Scheme 1) as it can increase the hydrophilic interaction by enhancing the polar character in the molecule.[19]

The dye is well-characterized by ^1H- and ^{13}C-NMR spectroscopy, single crystal X-ray diffraction, ESI-mass spectrometry and elemental analyses. It acts as a fluorescence turn-on chemosensor for the Al^{3+} ion in aqueous ethanol medium.

Experimental section

Materials and methods

Reagent grade rhodamine B and all metal perchlorate and nitrate salts were from Sigma Aldrich (USA). 2-Methoxy-4-nitroaniline was obtained from Alfa Aesar (USA). Other chemicals such as triethylamine, $POCl_3$ and EDTA were obtained from S. D. Fine Chemicals (India). These chemicals were used as received without further purification. All the solvents were from S. D. Fine Chemicals and were dried following standard protocols prior to use. Chromatographic separation was done by column chromatography using basic Al_2O_3 from S. D. Fine Chemicals (India).

Caution! Perchlorate salts are potentially explosive especially if they are mixed with organic solvents and should be handled with utmost care.

Analysis and measurements

Both ^1H NMR (500 MHz) and ^{13}C NMR (125 MHz) spectra of the compounds were recorded on a JEOL JNM-LA500 FT spectrometer in $CDCl_3$ with tetramethylsilane as the internal

[a]*Department of Chemistry, Indian Institute of Technology Kanpur, Kanpur 208016, India. E-mail: pkb@iitk.ac.in; Fax: +91-512-259-7637; Tel: +91-512-259-7034*

[b]*Cytogenetics and Molecular Biology Laboratory, Department of Zoology, University of Kalyani, Kalyani 741235, India*

[c]*Department of Zoology, Dumdum Motijheel College, West Bengal State University, Kolkata 700074, India*

† Electronic supplementary information (ESI) available: Materials and physical methods, general procedures, tables, schemes, figures, characterization data, and some spectra. CCDC 1421529. For ESI and crystallographic data in CIF or other electronic format see DOI: 10.1039/c5ra23968k

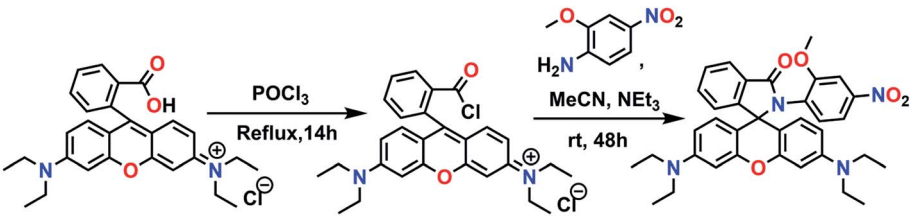

Scheme 1 Synthetic route of the chemosensor L.

standard. The ESI-mass data were obtained in acetonitrile using a WATERS-Q-TOF Premier Mass Spectrometer. UV-vis absorption spectra were recorded on a Shimadzu 2450 UV-vis spectrophotometer in aqueous ethanol medium at 298 K. Steady-state fluorescence spectra were obtained using a Perkin-Elmer LS 50B Luminescence spectrometer at 298 K with excitation and emission band-pass of 10 nm. The excitation wavelength was 520 nm and the spectra were recorded in the range 540–700 nm. Fluorescence quantum yields were determined by comparing the corrected spectra with that of pure rhodamine B in ethanol (ESI†).

Single-crystal X-ray data of compound **L** was collected at 100 K on a Bruker SMART APEX CCD diffractometer using graphite monochromated MoK$_\alpha$ radiation (λ = 0.71073 Å). The data reduction, structure solution and refinements were carried out using the SHELXL-97 package. The details are also provided in the ESI.†

Jobs plot and Benesi–Hildebrand plot

Job's plot experiment was conducted, keeping the total concentration of **L** and **L**–Al^{3+} complex at 1×10^{-4} mol L^{-1} and the mole fraction of Al^{3+} varied from 0 to 1. The sensor **L** (2.96 mg) was dissolved in 5 mL ethanol to make a solution of 10^{-3} M order and diluted to 25 mL 1.0×10^{-4} M order by addition of ethanol and water (EtOH : H_2O = 2 : 3, v/v). 2.7, 2.4, 2.1, 1.8, 1.5, 1.2, 0.9, 0.6 and 0.3 mL stock solution of **L** were taken and kept them into vials. 25 mL 1.0×10^{-4} M stock solution of $Al(NO_3)_3 \cdot 9H_2O$ was also prepared in similar way in ethanol. 0.3, 0.6, 0.9, 1.2, 1.5, 1.8, 2.1, 2.4 and 2.7 mL Al^{3+} stock solution were to the vials containing solution of sensor in such a way that total volume of each vial were 3 mL. After shaking the vials UV-vis absorbance were performed at room temperature.

Similarly for Benesi–Hildebrand experiment a series of stock solution of $Al(NO_3)_3 \cdot 9H_2O$ were prepared from 1×10^{-6} to 1×10^{-3} M range in different vials and added separately to 1×10^{-5} M solution of **L**. After mixing the vials fluorescence spectra were recorded at room temperature.

Cell culture and imaging

MTT [3-(4,5-dimethylthiazol-2-yl)-2,5-diphenyltetrazolium bromide] and dimethyl sulphoxide (DMSO) of analytical grade were procured from Sigma-Aldrich Inc. (St-Louis, MO, USA); Dulbecco's modified Eagle's medium (DMEM), fetal bovine serum, and antibiotics were procured from Gibco BRL (Grand Island, NY, USA). All organic solvents used were of HPLC grade. Briefly, the rat skeletal muscle cells of L6 cell line obtained from National Centre for Cell Science, Pune, India, were grown in Dulbecco's modified Eagle's Medium (DMEM) supplemented with 10% foetal bovine serum and 1% antibiotic in a 5% carbon dioxide incubator maintained at 37 °C and plated in different Petri-plates.[20] All the control and experimental sets of cells were grown till they attained 70–80% confluence, and then the different treatment procedures commenced. The concentration of the sensor optimized for the study was estimated at 7×10^{-5} M (20 mL of total volume of stock solution); it was incubated for 15 min and the concentration of that of $Al(NO_3)_3$ salt solution standardized at 4×10^{-3} M (5 mL of total volume of stock solution) was also incubated for 15 min. Cell images were taken under an Andor Spinning Disk Confocal Microscope. The images were then evaluated against untreated control set of cells. The fluorescence intensity profile was derived using Analysis Software, NIS Elements AR Version 4.00.

Synthesis of the chemosensor L

Synthesis of the chemosensor was easily achieved in two steps as illustrated in Scheme 1.

To rhodamine B (2 g, 4.2 mmol) taken in a three-necked round bottom flask, 50 mL of freshly distilled phosphorous oxychloride was added and the mixture was heated reflux for 24 h under a dinitrogen blanket. Excess $POCl_3$ was then distilled off and the acid chloride formed was dried under reduced pressure and used for the next step without further purification. The crude acid chloride was dissolved in dry acetonitrile (70 mL) and treated with 2-methoxy-4-nitroaniline (1.2 equivalents) in presence of triethylamine (2 mL) taken in the same solvent (50 mL) over a period of 20 min. After the addition was complete, the reaction mixture was allowed to stir at room temperature for 48 h and then all the solvent was removed under reduced pressure. The crude reaction mixture was dissolved in dichloromethane (3 × 50 mL) and washed several times with water. The organic layer after drying over anhydrous Na_2SO_4, was evaporated off completely to afford a dark pink solid. Column chromatography on basic Al_2O_3 using DCM/hexane (70 : 30, v/v) as the eluent provided the desired product as a pale yellow crystalline sold in ~58% yield. Mp ~ 210 °C (uncorrected); ^{1}H NMR (500 MHz, $CDCl_3$, 25 °C, $Si(CH_3)_4$) δ: 1.13 (t, 12H, J = 7.45 Hz), 3.29 (q, 8H, J = 6.85 Hz), 3.58 (s, 3H), 6.19 (d, 2H, J = 2.3 Hz), 6.29 (dd, 2H, J = 2.3, 8.75 Hz), 6.38 (d, 1H, J = 8.05 Hz), 6.65 (d, 2H, J = 8.55 Hz), 7.21 (s, 1H), 7.53–7.55 (m, 4H), 8.00–8.02 (m, 1H) (Fig. S1†); ^{13}C NMR (125 MHz, $CDCl_3$, 25 °C, $Si(CH_3)_4$) δ: 12.66, 44.44, 56.07, 68.38,

97.48, 105.76, 106.85, 107.68, 115.51, 123.59, 124.39, 128.47, 129.59, 129.72, 131.46, 131.92, 133.02, 147.99, 148.94, 152.89, 153.54, 156.56, 166.69 (Fig. S2†). ESI MS: *m/z* (%): 593.2761 (100) $[M + H^+]^+$ (Fig. S3†); anal. calcd for $C_{35}H_{36}N_4O_5$: C, 70.93; H, 6.12; N, 9.45%. Found: C, 71.07; H, 6.28; N, 9.32%.

Results and discussion

The chemosensor **L** can be synthesized from readily available chemicals in two steps. The rectangular parallelepiped pale yellow single crystals, suitable for X-ray crystallography were obtained by slow evaporation of the solution of the compound in ethyl acetate at room temperature. A perspective view of the molecule is shown in Fig. 1 while the crystallographic data are collected in Table S1 in the (ESI†).

Photophysical properties

The probe is readily soluble in common organic solvents and also has sufficient solubility in aqueous-organic medium. All spectroscopic measurements were carried out in aqueous ethanol (EtOH–H_2O, 2 : 3 v/v) medium. Perchlorate salts of metal ions that include Na^+, K^+, Mg^{2+}, Ca^{2+}, Mn^{2+}, Fe^{2+}, Fe^{3+}, Co^{2+}, Ni^{2+}, Cu^{2+}, Zn^{2+}, Cd^{2+}, Ag^+, Pb^{2+} and Hg^{2+} were used in the photophysical studies. For Al^{3+} and Cr^{3+} ions nitrate salts were used. The metal free dye **L** exhibits negligible absorption and fluorescence above 500 nm implies the retention of the spirolactam bond in this region. However, addition of 10 equivalents of the Al^{3+} ion to a solution of **L** makes the solution from colorless to pink in about 20 min that can be detected with a naked eye. In the visible region, a strong band appears at 565 nm with a shoulder around 525 nm (Fig. 2) indicating breaking of the spirolactam bond in presence of the Al^{3+} ion. No such significant change is observed in presence of any of the aforementioned metals ions.

Upon excitation at 520 nm, the metal-free chemosensor **L** ($\Phi = 0.0065$) exhibit only a very weak fluorescence. In sharp contrast, addition of Al^{3+} ion to the solution of **L** leads to a strong emission (~50 fold enhancement) giving a band centering around 580 nm ($\Phi = 0.328$) (Fig. 3).

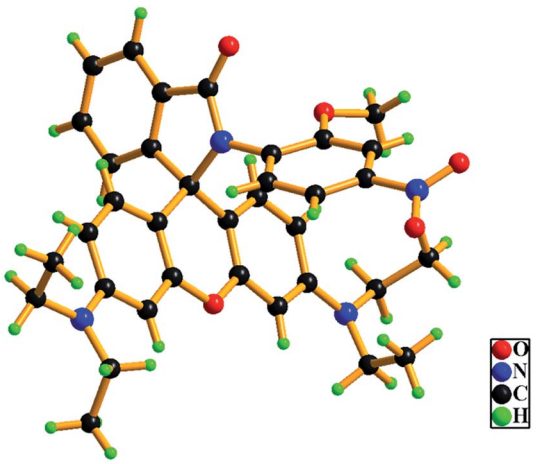

Fig. 1 X-ray single crystal structure of **L**.

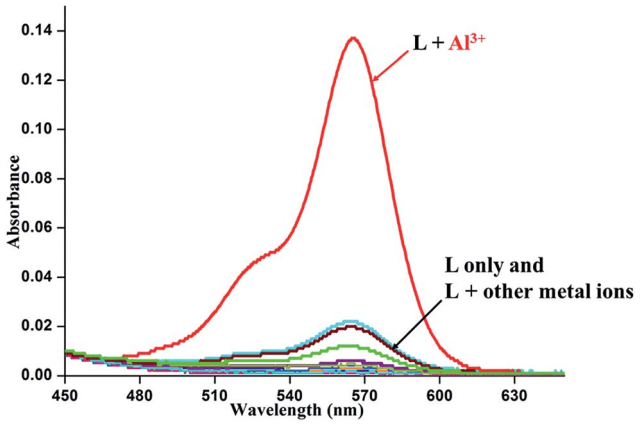

Fig. 2 Absorption spectra of **L** in EtOH–H_2O (2 : 3, v/v) medium in the presence of 10 equivalents of metal ions. [**L**] = 1×10^{-4} M.

Other metal ions listed above do not elicit any noticeable emission when added to the solutions of **L**. These results are consistent with the absorption spectral results. To confirm the spirocyclic ring opening, the ^{13}C NMR spectra of the complexes were also recorded. The absence of the characteristic peak of the quaternary carbon in the region, 67.0–69.0 ppm (ref. 21 and 22) in the metal complex (Fig. S4†) reveals the rupture of the spirolactam bond to the ring-open form. In the IR spectra of the metal free sensor **L** the amide carbonyl frequency appears at 1709 cm^{-1}. The downward shift around 1589 cm^{-1} (Fig. S5†) of the amide carbonyl stretching in the complexes is consistent with fact that the carbonyl oxygen is involved in the coordination. In addition, a peak in the region 1370–1384 cm^{-1} suggests the presence of coordinated nitrate ion (NO_3^-) in the complex.

Theoretical study

For better understanding about the nature of binding of the ligands, theoretical calculations were performed using Gaussian-09 software. For the comparative study, various

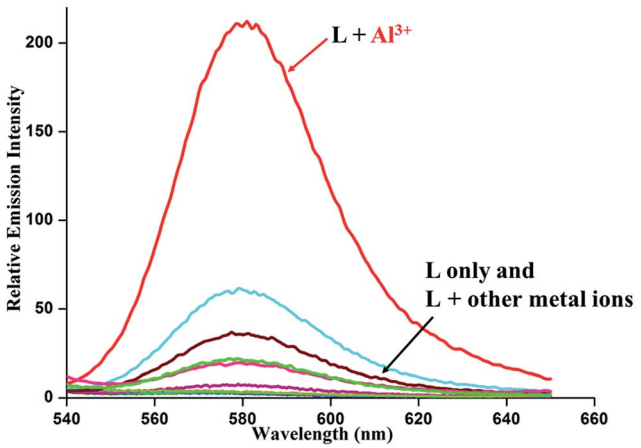

Fig. 3 Relative emission spectra of **L** in EtOH–H_2O (2 : 3, v/v) in presence of 10 equivalents of metal ions. [**L**] = 10 μM. Slit width = 10/10 nm. λ_{ex} = 520 nm.

molecular interactions of the ligand **L** and **L**–Al^{3+} complex has been studied using density functional theory (DFT) with the B3LYP/6-31G (d,p+) functional model and basis set. Energy optimization calculations have revealed that **L**–Al^{3+} complex is energetically much more stable compared to the ligand **L**. Here the energy gap between the HOMO and LUMO of the complex (2.28 eV) was less compared to that of the corresponding sensor **L** (2.79 eV) (Fig. 4).

From the spatial electronic distribution in the frontiers orbitals of the ligand **L** it can be easily pointed out that in the free ligand the electron density mainly resides on the xanthene moiety and some electron clouds on C=O moiety. In the complexes, spirolactam bonds were opened when the Al^{3+} ions bind to the ligand. These structural change introduced by the attachment of the metals ions lead to significant charge transfer from the xanthene moiety towards the metal binding moiety that could be well observed from the frontiers orbitals of the complex. Here the electron charge cloud was pulled towards the electron withdrawing nitro group in the LUMO. So here the extent of these transfer of electron cloud have played crucial role to this tuning of selectivity towards the tripositive ions. The optimized structures of the sensor **L** and **L**–Al^{3+} complexes are summarized in Fig. S9.†

Selectivity experiment

In order to check the selectivity of **L** towards Al^{3+} ions over the other tested metal ions competitive studies were carried out (Fig. 5). The emission responses of the sensor **L** towards Al^{3+} ion in the presence of excess of background metal ions are also recorded. In presence of other competing metal ions, no significant change in the emission intensity has been noticed in the sensing of Al^{3+} ion confirming its selectivity towards the Al^{3+} ion.

The binding stoichiometry was determined by the Job's plot experiments based on absorption keeping the total concentration of **L** and Al^{3+} ion at 1×10^{-4} M (Fig. 6).[23] The experiments

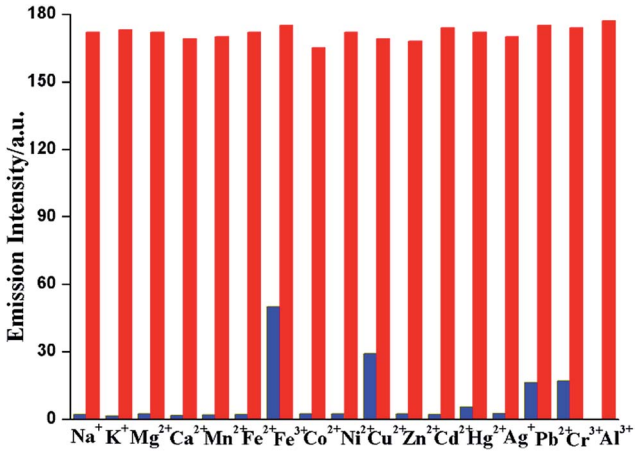

Fig. 5 Selectivity of the dye L for Al^{3+} ion in EtOH–H_2O (2 : 3, v/v) mixture. Blue bars indicate the fluorometric response of L with 50 equivalents of the metal ion of interest; red bars represent the final integrated fluorescence response after the addition of 10 equivalents of Al^{3+} ion to each solution containing other metals over the initial integrated emission. Dye concentration = 10 μM; λ_{exc} = 520 nm.

support 1 : 1 complexation between **L** and Al^{3+}. A peak at 743.3220 due to $[\mathbf{L} + Al^{3+} + 2NO_3^-]^+$ in the ESI-mass spectrum of the Al^{3+} complex further confirms this 1 : 1 binding stoichiometry (Fig. S6†).

The association constant for the complex and the detection limit were determined from emission titration data (Fig. 7).[24] Following the Benesi–Hildebrand plot[25] the association constant of **L** with Al^{3+} ion is found to be 6.53×10^3 M^{-1} (R^2 = 0.99496) (Fig. 8a). This value matches well with the reported range (10^3 to 10^9 M^{-1}) of the association constants for the Al^{3+} specific chemosensors reported in the literature.[26,27] The detection limit is calculated to be 0.316 μM (Fig. 8b) which is smaller compared to the maximum concentration of 7.41 μM of Al^{3+} ion in drinking water approved by WHO.[28] Also the calculated value of detection limit is found to lie in comparable range (1.0×10^{-6} M) for the reported Al^{3+} sensors.[13,29–34]

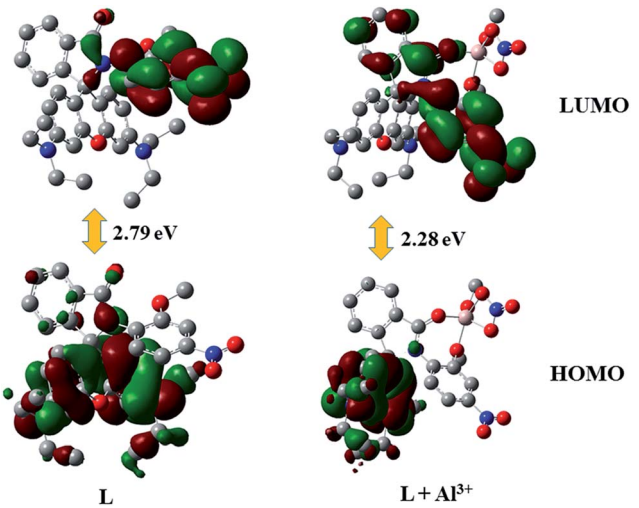

Fig. 4 Optimized structures of HOMO and LUMO of the ligand L and L–Al^{3+} complex.

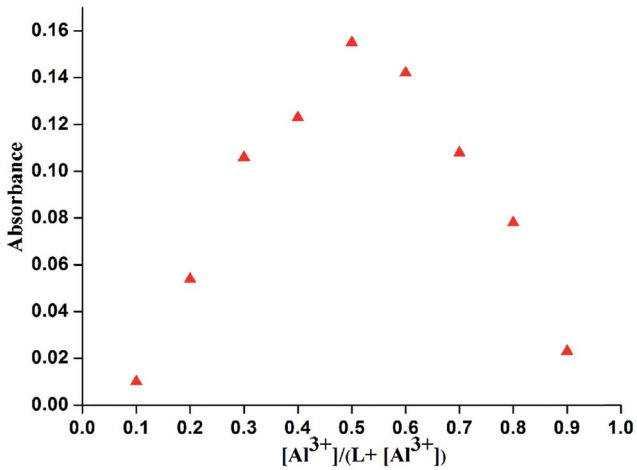

Fig. 6 Job's plot of absorbance of L and Al^{3+} in EtOH–H_2O (2 : 3, v/v) medium. Total concentration = 1×10^{-4} M.

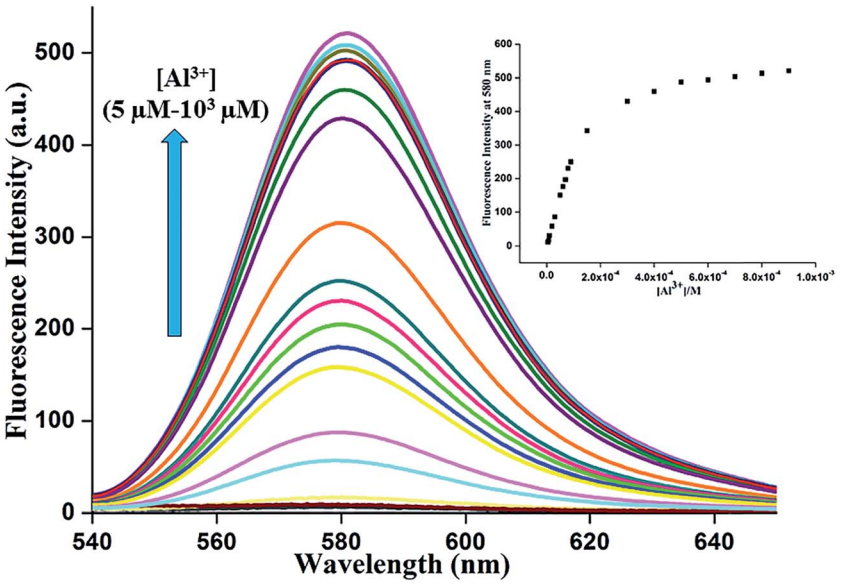

Fig. 7 Change of fluorescence spectra of the dye L as a function of [Al^{3+}] ion in neutral EtOH–H_2O (2 : 3 v/v) medium. The arrow indicates the trend in increasing [Al^{3+}].

Reversibility of fluorescence is an imperative characteristic in developing chemosensors for practical aspects. The reversible nature of the sensor **L** is checked by adding an aqueous solution of Na_2EDTA to the solution of metal complex. Addition of excess EDTA salt solution results in the lowering of emission intensity to the levels of metal-free sensors (Fig. 9).

Cell imaging studies

The potentiality of a sensor to determine the presence of guest species in living cells is of immense practical importance.[35] To confirm the competence of the chemosensor in biological samples the intracellular confocal imaging studies have been carried out in the presence of Al^{3+} ion. No distinct intracellular fluorescence was observed for the series of cells incubated with normal untreated cells (B) or sensor (H) alone. However, significant increase in the fluorescence was gradually observed in case of sensor **L** when exogenous Al^{3+} stock solution was added into them *via* incubation with $Al(NO_3)_3$ salt solution (N) (Fig. 10). This finding corroborated well with the statistically analyzed fluorescence intensity profile (Fig. S7†). Counter-staining of the cells was also done with Hoechst dye to confirm the permeability range of the sensors which showed a more prominent distribution in the cytoplasm than that of the nucleus (Fig. 10).

MTT assay for cell viability assessment

For the sensor **L**, the MTT assay (Mosmann, 1983) has been performed to evaluate the extent of cytotoxicity it could induce in normal cells.[36] The cell viability sustains ~85–90% upon treatment of maximum dose of **L** (50 μL of stock solution),

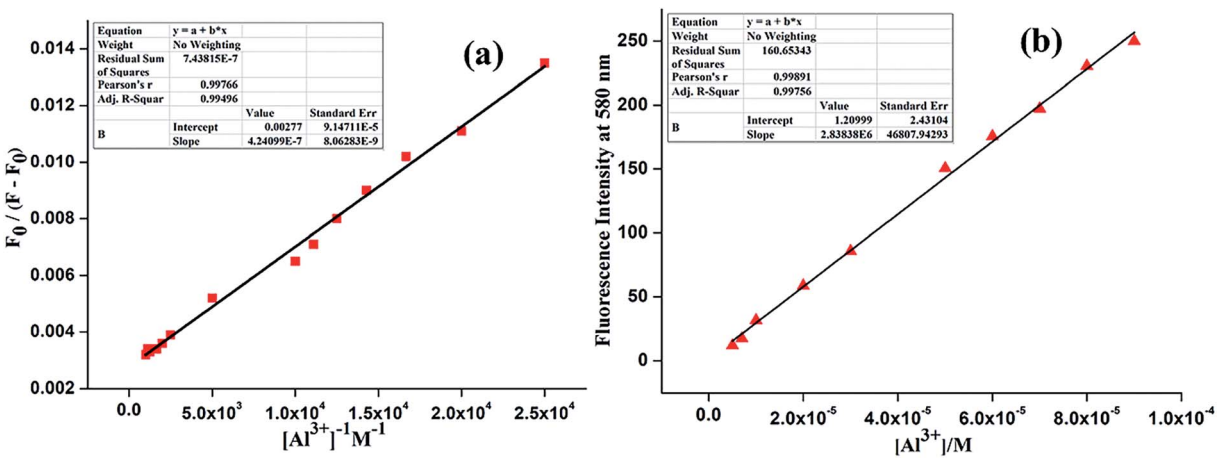

Fig. 8 (a) Binding constant plot of L for Al^{3+}. (b) Linear response curve of L at 580 nm depending on the Al^{3+} ion concentration for determination of lowest detection limit.

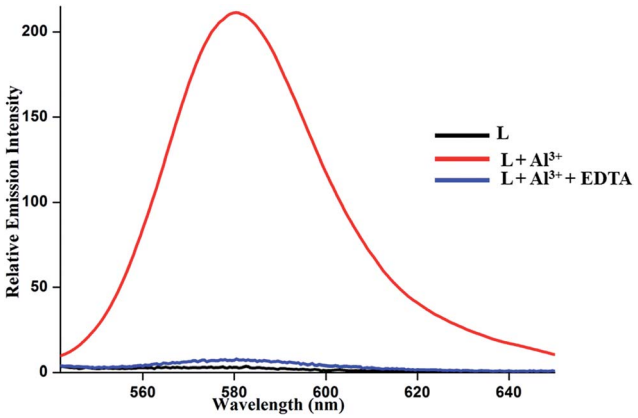

Fig. 9 Emission responses of **L** in the presence of 10 equivalents Al^{3+} ion and subsequent addition of excess EDTA solution to the **L** complex of Al^{3+} ion in EtOH–H_2O (2 : 3, v/v) medium.

which indicates that the sensor **L** does not affect the cell viability to a significant extent, an important criterion for biological application and also supports the intracellular Al^{3+} ion detection in living cells as well. No significant difference was observed between the percentages of viable cells in the sensor-treated and the solvent-treated lots, indicating thereby that the sensors were non-cytotoxic and safe for biological uses (Fig. S8†).

Conclusions

In summary, a new rhodamine based chemosensor **L** has been synthesized readily. Metal assisted spirolactam ring opening of the dyes give noticeable change in fluorescence response. Sufficient water solubility, high selectivity, sensitivity, reversibility along with the noticeable color change made this probes suitable chemosensor for the Al^{3+} ion. The sensor **L** being non-

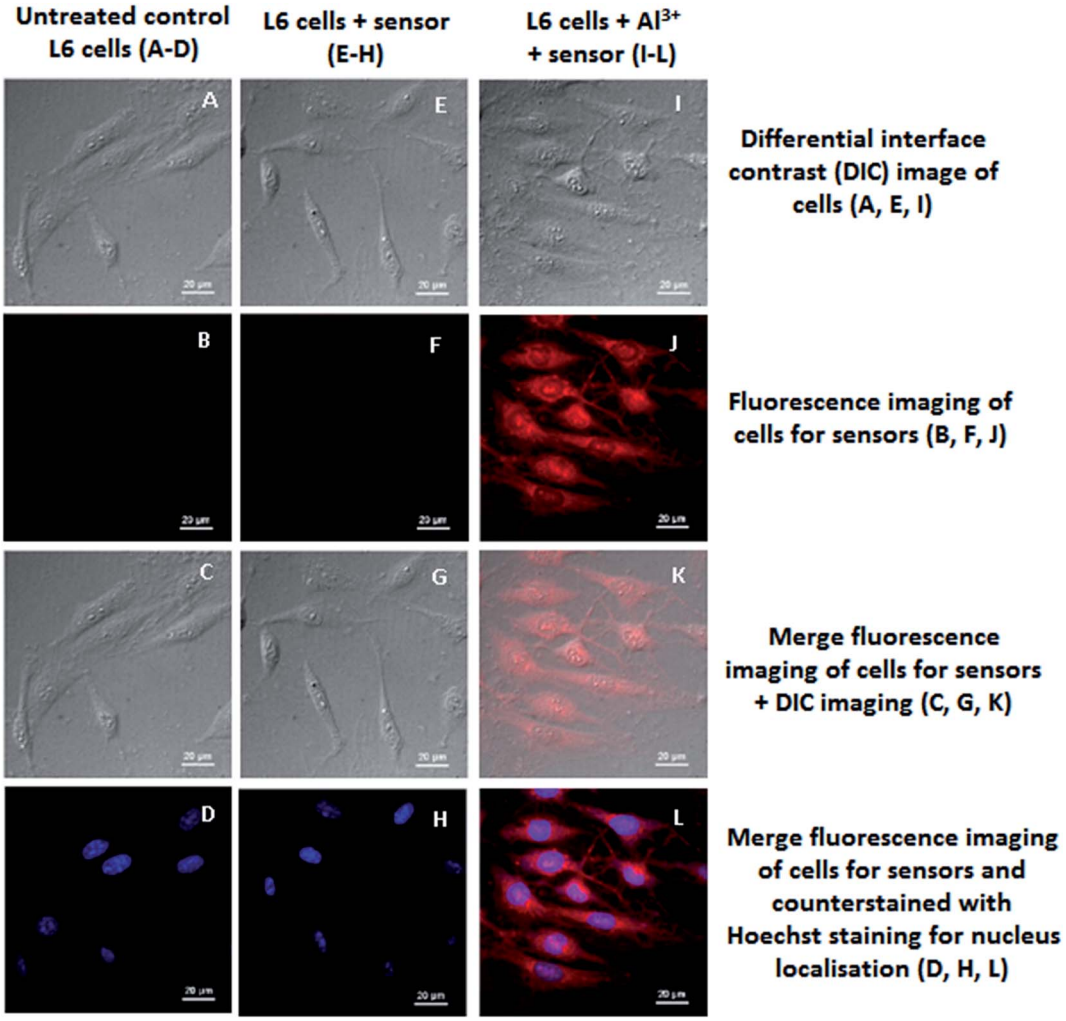

Fig. 10 Confocal imaging of control and treatment series of L6 cells for sensor **L** viewed under 40× magnification; the scale bar provided in each image measures 20 μm in size: (A–D) Untreated control L6 cells; (E–H) L6 cells + sensor; (I–L) L6 cells + Al^{3+} + sensor; differential interface contrast (DIC) image of untreated control L6 cells (A), L6 cells + sensor (E) and L6 cells + Al^{3+} + sensor (I); fluorescence imaging of untreated control L6 cells (B), L6 cells + sensor (F) and L6 cells + Al^{3+} + sensor (J); merge fluorescence imaging + DIC imaging of untreated control L6 cells (C), L6 cells + sensor (G) and L6 cells + Al^{3+} sensor (K); merge fluorescence imaging of cells for sensors and Hoechst staining for nucleus localisation of untreated control L6 cells (D), L6 cells + sensor (H) and L6 cells + Al^{3+} + sensor (L).

cytotoxic in nature, and having easy cellular penetrability can be a possible candidate for some practical application as an additional tool for detection of cellular Al^{3+} ions.

Acknowledgements

This work was supported by Department of Science and Technology, New Delhi, India (SERB/CHM/20130239). PKB thanks SERB for the funding. Financial support from the CSIR, New Delhi to NC and PM are gratefully acknowledged. SBM thanks IIT Kanpur for financial assistance. ARK-B and AS sincerely thank to UGC, New Delhi for awarding an Emeritus Fellowship. The authors are thankful to Department of Zoology, The University of Kalyani.

Notes and references

1 K. P. Carter, A. M. Young and A. E. Palmer, *Chem. Rev.*, 2014, **114**, 4564–4601.
2 D. T. Quang and J. S. Kim, *Chem. Rev.*, 2010, **110**, 6280–6301.
3 J. P. Desvergne and A. W. Czarnik, Chemosensors of Ion and Molecule Recognition, in *NATO Science Series C: Mathematical and Physical Sciences*, Kluwer Academic, Dordrecht, London, 1997.
4 S. Kim, J. Y. Noh, K. Y. Kim, J. H. Kim, H. K. Kang, S. W. Nam, S. H. Kim, S. Park, C. Kim and J. Kim, *Inorg. Chem.*, 2012, **51**, 3597–3602.
5 D. Maity and T. Govindaraju, *Inorg. Chem.*, 2010, **49**, 7229–7231.
6 S. W. King, J. Savory and M. R. Willis, *Crit. Rev. Clin. Lab. Sci.*, 1981, **13**, 1–20.
7 I. Shcherbatykh and D. O. Carpenter, *J. Alzheimer's Dis.*, 2007, **11**, 191–205.
8 E. Delhaize and P. R. Ryan, *Plant Physiol.*, 1995, **107**, 315–321.
9 X. Chen, T. Pradhan, F. Wang, J. S. Kim and J. Yoon, *Chem. Rev.*, 2012, **112**, 1910–1956.
10 J. R. Lakowicz, *Principles of Fluorescence Spectroscopy*, Springer, New York, 3rd edn, 2006.
11 S. Pal, N. Chatterjee and P. K. Bharadwaj, *RSC Adv.*, 2014, **4**, 26585–26620.
12 S. B. Maity and P. K. Bharadwaj, *Inorg. Chem.*, 2013, **52**, 1161–1163.
13 I. H. Hwang, Y. W. Choi, K. B. Kim, G. J. Park, J. J. Lee, L. Nguyen, I. Noh and C. Kim, *New J. Chem.*, 2016, **40**, 171–178 and references 21–61 therein.
14 B. Sen, M. Mukherjee, S. Banerjee, S. Pal and P. Chattopadhyay, *Dalton Trans.*, 2015, **44**, 8708–8717 and references therein.
15 K. Ghosh, A. Majumdar and T. Sarkar, *RSC Adv.*, 2014, **4**, 23428–23432.
16 S. Sahana, S. Bose, S. K. Mukhopadhyay and P. K. Bharadwaj, *J. Lumin.*, 2016, **169**, 334–341.
17 Y.-W. Wang and Y. Peng, *Org. Lett.*, 2012, **14**, 3420–3423.
18 S. Gui, Y. Huang, F. Hu, Y. Jin, G. Zhang, L. Yan, D. Zhang and R. Zhao, *Anal. Chem.*, 2015, **87**, 1470–1474 and references therein.
19 L. Di and E. Kerns, *Drug-Like Properties: Concepts, Structure Design and Methods from ADME to Toxicity Optimization*, Elsevier Science, London, 2nd edn, 2015, pp. 61–90.
20 A. Samadder, S. Das, J. Das and A. R. Khuda-Bukhsh, *Colloids Surf., B*, 2013, **109**, 10–19.
21 S. Saha, M. U. Chhatbar, P. Mahato, L. Praveen, A. K. Siddhanta and A. Das, *Chem. Commun.*, 2012, **48**, 1659–1661.
22 K. Ghosh, T. Sarkar and A. Samadder, *Org. Biomol. Chem.*, 2012, **10**, 3236–3243.
23 C. Yang, L. Liu, T.-W. Mu and Q.-X. Guo, *Anal. Sci.*, 2000, **16**, 537–539.
24 J. Bourson, J. Pouget and B. Valeur, *J. Phys. Chem.*, 1993, **97**, 4552–4557.
25 H. A. Benesi and J. H. Hildebrand, *J. Am. Chem. Soc.*, 1949, **71**, 2703–2707.
26 D. Maity and T. Govindaraju, *Chem. Commun.*, 2010, **46**, 4499–4501.
27 S. H. Kim, H. S. Choi, J. Kim, S. J. Lee, D. T. Quang and J. S. Kim, *Org. Lett.*, 2010, **12**, 560–563.
28 *Guidelines for drinking-water quality*, World Health Organization, Health criteria and other supporting information, Geneva, 2nd edn, 1996, vol. 2.
29 W.-H. Ding, D. Wang, X.-J. Zheng, W.-J. Ding, J.-Q. Zheng, W.-H. Mu, W. Cao and L.-P. Jin, *Sens. Actuators, B*, 2015, **209**, 359–367.
30 J. Kumar, M. J. Sarma, P. Phukan and D. K. Das, *Dalton Trans.*, 2015, **44**, 4576–4581.
31 Y. Fu, X.-J. Jiang, Y.-Y. Zhu, B.-J. Zhou, S.-Q. Zang, M.-S. Tang, H.-Y. Zhang and T. C. W. Mak, *Dalton Trans.*, 2014, **43**, 12624–12632.
32 M. Shellaiah, Y. H. Wu and H. C. Lin, *Analyst*, 2013, **138**, 2931–2942.
33 V. P. Singh, K. Tiwari, M. Mishra, N. Srivastava and S. Saha, *Sens. Actuators, B*, 2013, **82**, 546–554.
34 Y.-Y. Guo, L.-Z. Yang, J.-X. Ru, X. Yao, J. Wu, W. Dou, W.-W. Qin, G.-L. Zhang, X.-L. Tang and W.-S. Liu, *Dyes Pigm.*, 2013, **99**, 693–698.
35 X. Peng, J. Du, J. Fan, J. Wang, Y. Wu, J. Zhao, S. Sun and X. Xu, *J. Am. Chem. Soc.*, 2007, **129**, 1500–1501.
36 T. Mosmann, *J. Immunol. Methods*, 1983, **65**, 55–63.